

Orbital signatures of Fano-Kondo line shapes in STM adatom spectroscopy

Sebastian Frank and David Jacob

Max-Planck-Institut für Mikrostrukturphysik, Weinberg 2, 06120 Halle, Germany

(Received 28 September 2015; published 15 December 2015)

We investigate the orbital origin of the Fano-Kondo line shapes measured in STM spectroscopy of magnetic adatoms on metal substrates. To this end we calculate the low-bias tunnel spectra of a Co adatom on the (001) and (111) Cu surfaces with our density functional theory-based *ab initio* transport scheme augmented by local correlations. In order to associate different d orbitals with different Fano line shapes we only correlate individual $3d$ orbitals instead of the full Co $3d$ shell. We find that Kondo peaks arising in different d levels indeed give rise to different Fano features in the conductance spectra. Hence, the shape of measured Fano features allows us to draw some conclusions about the orbital responsible for the Kondo resonance, although the actual shape is also influenced by temperature, effective interaction, and charge fluctuations. Comparison with a simplified model shows that line shapes are mostly the result of interference between tunneling paths through the correlated d orbital and the sp -type orbitals on the Co atom. Very importantly, the amplitudes of the Fano features vary strongly among orbitals, with the $3z^2$ orbital featuring by far the largest amplitude due to its strong direct coupling to the s -type conduction electrons.

DOI: [10.1103/PhysRevB.92.235127](https://doi.org/10.1103/PhysRevB.92.235127)

PACS number(s): 73.63.-b, 72.10.Fk

I. INTRODUCTION

The Kondo effect is one of the most fascinating phenomena in condensed matter physics, occurring in a vast number of different systems (see, e.g., Ref. [1] and references therein), ranging from bulk metals doped with magnetic impurities [2–4] to nanoscale systems such as semiconductor quantum dots [5,6] and carbon nanotubes connected to metal leads [7,8]. Generally, the Kondo effect leads to the quenching of a local magnetic moment associated with localized and strongly interacting electronic states in the system by interaction with the conduction electrons. The quenching of the spin is accompanied by drastic changes in the electronic and transport properties. This strong impact on the electronic and magnetic properties of a system makes the Kondo effect an important factor for the functionality of atomic and molecular-scale electronic devices.

Since the pioneering works of Li *et al.* [9] and Madhavan *et al.* [10] scanning tunneling spectroscopy (STS) has become a standard tool for probing the Kondo effect of magnetic adatoms and molecules on metallic substrates [11–18]. The Kondo effect arises from the interaction of the magnetic moment of the adsorbate with the conduction electrons of the metal surface and leads to the screening of the magnetic moment by formation of a total spin singlet state with the conduction electrons. The formation of the Kondo-singlet state is signaled by the appearance of a strongly renormalized quasiparticle peak at the Fermi level, the so-called Abrikosov-Suhl or Kondo resonance. In STS the appearance of the Kondo peak in the local DOS of the atom or molecule leads to a zero-bias anomaly (ZBA) in the tunnel spectra, which is generally well described by a Fano line shape [19], although it has recently been found that the ZBAs are actually much better described in terms of generalized Frota line shapes [20] as the Frota function yields a much better description of the Kondo peak than the Lorentz function [21,22].

The origin of the Fano-like line shape is either understood as due to the interference of different tunneling paths—one via the strongly interacting orbitals of the magnetic

atom bearing the sharp Kondo resonance, and others going directly to the substrate [23–25]—or is explained in terms of tunneling into the surface alone [26–30]. A recent study [31] combines density functional theory (DFT) with numerical renormalization group (NRG) calculations and determines the line shape by looking at energy-dependent transmission eigenvalues. Surprisingly, no systematic study of the relation between orbital symmetry of the orbital(s) bearing the Kondo resonance and the shape of the resulting Fano resonances has been conducted so far.

In this paper, we intend to close this gap by calculating the Fano line shapes corresponding to Kondo peaks appearing in different orbitals of the $3d$ shell of a magnetic atom on metal surfaces. To this end we select individual d orbitals and perform *ab initio* quantum transport calculations augmented by local correlations for the selected d orbital only. There is merit in doing so: Even in a multiorbital situation the Kondo effect is signaled by Kondo peaks in individual d orbitals, and often the Fano-Kondo feature of one d orbital will be dominant in the tunnel spectrum due to different tunneling matrix elements and Kondo scales.

We choose to study Co@Cu(001) and Co@Cu(111) as our test systems, which have been extensively studied theoretically and experimentally [12,18,25,28–34]. We find that Kondo peaks arising in different d levels indeed give rise to different Fano features in the conductance spectra. However, temperature, effective interaction, and occupancy of the d orbital also play an important role. With one notable exception, a simplified two-level model consisting of the d orbital bearing the Kondo resonance and one s or p orbital on the adatom accounts for the calculated line shapes. This shows that in these cases tunneling into substrate states only plays a minor role for determining the actual line shapes.

The paper is organized as follows: In Sec. II we briefly describe the method for calculating the zero-bias anomalies in the conductance spectra corresponding to Kondo peaks in different orbitals. In Sec. III we introduce two types of Fano line shapes: the standard one based on a Lorentzian resonance for the localized state and one based on the Frota

line shape better suited for describing the Kondo resonance. In Sec. IV we present results for a Co adatom placed on a Cu(001) and a Cu(111) surface, respectively. In Sec. V we devise a simplified model capturing the essence of the different situations encountered for different orbital symmetries and discuss the obtained results in the context of this model. In Sec. VI, a more general discussion follows relating our results to other experimental and theoretical works. Finally, in Sec. VII, we conclude this work with some general remarks on the significance of our results for other atomic or molecular Kondo systems.

II. METHOD

We consider a magnetic atom (here, Co) that is placed on a metallic substrate (here, Cu(001) or Cu(111)). A Cu STM tip is placed directly above the Co atom 6 Å away so that we are in the tunneling regime. The system is divided into three parts as shown in Fig. 1: two metal leads, S and T, representing the bulk electrodes connected to the substrate and STM tip, respectively, and the device region (D), which contains the magnetic atom and part of the surface and the STM tip.

We perform DFT-based *ab initio* quantum transport calculations using the ANT.G package [35]: The electronic structure of the D region is calculated on the level of Kohn-Sham (KS) DFT employing the LSDA functional [36] in the SVWN parametrization [37,38] and a minimal Gaussian basis set including the valence ($4s4p3d$) and outer core electrons ($3s3p$) of the Co and Cu atoms [39–43]. The effect of the bulk electrodes S and T, which are modeled by Bethe lattices [44], on the electronic structure of D is taken into account via self-energies $\hat{\Sigma}_S$ and $\hat{\Sigma}_T$. The KS Green's function (GF) of the D region is thus given by

$$\hat{G}_D^0(\omega) = [(\omega + \mu)\hat{P}_D - \hat{H}_D^0 - \hat{\Sigma}_T(\omega) - \hat{\Sigma}_S(\omega)]^{-1}, \quad (1)$$

where μ is the chemical potential, \hat{P}_D the projection operator onto D, and \hat{H}_D^0 is the KS Hamiltonian of the D region.

In order to capture Kondo physics, electronic correlation beyond conventional DFT have to be included. This is done

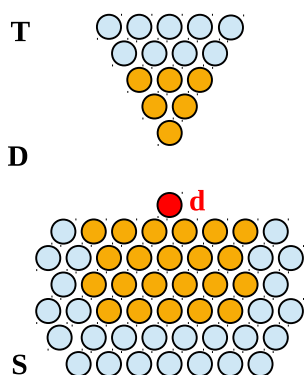


FIG. 1. (Color online) Schematic drawing of an STM tip probing a magnetic atom on a metal substrate. The system is separated into three parts: the device region D (gray/yellow) contains the magnetic atom (dark gray/red) hosting the d orbital giving rise to the Kondo peak, and parts of the substrate and STM tip. T and S (light gray/blue) are the bulk electrodes connected to the STM tip and substrate, respectively.

by combining DFT with the one-crossing approximation (OCA) [45], following the scheme developed in previous work [46,47]. In contrast to previous work, we are interested in the Kondo signatures of specific d orbitals, and not of the entire $3d$ shell.

Hence, we add a Hubbard-like interaction term $\hat{\mathcal{H}}_U = U\hat{n}_{d\uparrow}\hat{n}_{d\downarrow}$ only to a *single* d orbital of the Co $3d$ shell, where $n_{d\sigma}$ is the number operator for the d orbital and a spin σ . Since the Coulomb interaction in the correlated d orbital has already been taken into account on a mean-field level in the KS-DFT calculation, a double-counting correction (DCC) term has to be subtracted from the KS Hamiltonian projected onto the d orbital $\epsilon_d^0 = \langle d|\hat{H}_D^0|d\rangle$:

$$\epsilon_d = \epsilon_d^0 - \epsilon_{dc}. \quad (2)$$

In contrast to previous work, the DCC is chosen such that a certain occupancy is achieved, i.e., for achieving particle-hole (ph) symmetry ($n_d = 1$) we choose ϵ_{dc} such that $\epsilon_d = -U/2$. Note that ph symmetry is only approximately achieved since the coupling of the d orbital to the rest of the system (see below) is generally not ph symmetric.

The interacting d orbital coupled to the electronic bath given by the rest of the system (i.e., substrate and tip) defines an Anderson impurity model (AIM) [48]. An effective description of the coupling of the d orbital to the bath is given by the so-called hybridization function $\Delta_d(\omega)$, which can be obtained from the KS GF by

$$\Delta_d(\omega) = \omega + \mu - \epsilon_d^0 - [G_d^0(\omega)]^{-1}, \quad (3)$$

where G_d^0 is the KS GF projected onto the d orbital, i.e., $G_d^0 = \langle d|\hat{G}_D^0|d\rangle$. The imaginary part of Δ_d yields the broadening Γ_d of the d orbital due to the coupling to the rest of the system.

The AIM is now solved in the OCA [45]. The solution yields the self-energy $\Sigma_d(\omega)$ describing the dynamic correlations of the d orbital. The correlated GF of the d orbital is then given by

$$G_d(\omega) = ([G_d^0(\omega)]^{-1} - \Sigma_d(\omega) + \epsilon_{dc})^{-1}. \quad (4)$$

Its imaginary part yields the spectral function or LDOS of the d orbital $\rho_d(\omega) = -\text{Im}G_d(\omega)/\pi$. Correspondingly, we obtain the correlated GF for the D region as

$$\hat{G}_D(\omega) = \{[\hat{G}_D^0(\omega)]^{-1} - (\Sigma_d - \epsilon_{dc})\hat{P}_d\}^{-1}. \quad (5)$$

This allows us to calculate the transmission function using the Caroli expression [49],

$$T(\omega) = \text{Tr}[\hat{G}_D\hat{\Gamma}_T\hat{G}_D^\dagger\hat{\Gamma}_S], \quad (6)$$

where the coupling matrices for the leads are defined by

$$\hat{\Gamma}_{T/S} = i(\hat{\Sigma}_{T/S} - \hat{\Sigma}_{T/S}^\dagger). \quad (7)$$

The self energies $\Sigma_{T/S}$ are typically symmetric, so that the coupling matrices are twice the imaginary part of the self energies. For low temperature and small-bias voltages, current and conductance can be related to the transmission function using the Landauer formula [50,51]. For the typical STM setup considered here most of the applied bias voltage drops at the

STM tip. In that case the conductance is simply given by

$$G(V) = \frac{2e^2}{h} T(eV). \quad (8)$$

We note that the use of the Landauer formula for the conductance is justified in the limit of small bias voltages compared to the Kondo temperature. In this limit transport occurs via the Kondo resonance and thus is essentially one-body like (apart from renormalization) and phase coherent so that the full nonequilibrium expression for transport through an interacting region given by Meir-Wingreen reduces to the simpler Landauer result [52]. For larger bias voltages, deviations from the Landauer result can occur [53–55], and one would have to make use of the Meir-Wingreen equation [52], which requires the solution of the AIM out of equilibrium.

III. FANO-LORENTZ AND FANO-FROTA LINE SHAPES

Fano line shapes or resonances, originally introduced by Fano in the context of autoionization and elastic electron scattering by helium [19], generally arise in resonant scattering processes due to quantum interference between a quasidecrete resonant state and a broad background continuum. The interference leads to an asymmetric line shape in the scattering cross section at energies close to the resonance energy that is well described by the Fano function

$$f(\epsilon) \propto \frac{(q + \epsilon)^2}{\epsilon^2 + 1}, \quad (9)$$

where the parameter q controls the shape of the Fano function, and ϵ is the energy with respect to the resonant level. Equation (9) can also be obtained from the complex representation of a Lorentzian multiplied by a phase factor $e^{i\phi_q}$

$$\rho_{\text{FL}}(\omega) = \text{Im} \left[e^{i\phi_q} \left(\frac{A}{\omega - \omega_0 + i\Gamma} \right) \right] + \rho_0, \quad (10)$$

where A is the amplitude, Γ is the half-width of the Lorentzian, ω_0 the resonance energy, and ρ_0 a constant offset. Using $q = \tan(\phi_q/2)$, $\epsilon = (\omega - \omega_0)/\Gamma$, and some algebra, this Fano-Lorentz (FL) line shape can be shown to be equivalent to the original Fano formula (see the Appendix):

$$\rho_{\text{FL}}(\omega) = \frac{A}{\Gamma} \left[\frac{(q + \epsilon)^2}{\epsilon^2 + 1} - 1 \right] \frac{1}{1 + q^2} + \rho_0. \quad (11)$$

STM spectroscopy of Kondo impurities presents a similar situation: The STM tip probes the continuous conduction electron density of states which interacts with the Kondo resonance at the Fermi level. The interference of different tunneling paths then leads to Fano-type line shapes in the conductance spectra. Assuming a Lorentzian form for the Kondo resonance naturally leads to Fano-Lorentz line shapes given by Eq. (11). However, in Refs. [21] and [22] Frota showed that the Kondo peak is actually better described by a line shape now known as a Frota line shape:

$$\rho_{\text{Frota}}(\omega) = \text{ARE} \left[\sqrt{\frac{i\Gamma_F}{\omega - \omega_0 + i\Gamma_F}} \right], \quad (12)$$

where the Frota parameter Γ_F is related to the actual half-width Γ of the resonance by $\Gamma \sim 2.54\Gamma_F$. A is the amplitude and ω_0

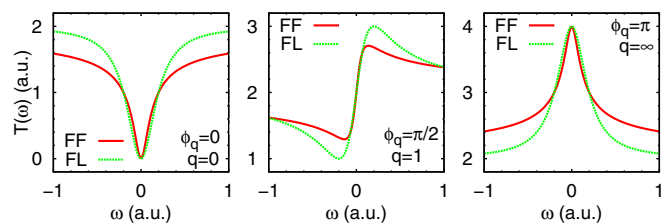


FIG. 2. (Color online) Comparison of Fano-Frota and Fano-Lorentz line shapes for different values of the q parameter but for identical amplitudes and half-widths.

the position of the Frota resonance. In analogy with Eq. (10) we define a Fano-Frota (FF) line shape as a generalized Frota curve [56] for describing the transmission function close to the Kondo resonance:

$$T_{\text{FF}}(\omega) = -A \text{Re} \left[e^{i\phi_q} \sqrt{\frac{i\Gamma_F}{\omega - \omega_0 + i\Gamma_F}} \right] + T_0. \quad (13)$$

The phase ϕ_q has the same meaning in the Lorentz and in the Frota case: A value of $\phi_q = 0$ leads to a dip, $\phi_q = \pi$ to a peak, and $\phi_q = \pi/2$ to a symmetric Fano line shape. In Fig. 2, we compare Fano-Frota and Fano-Lorentz features, choosing identical amplitudes and half-widths. Note that for the same half-width Frota line shapes have a slower decay than the Lorentzian ones.

In Fig. 3, we show FL and FF fits to the Kondo peak (left) in the calculated spectral function $\rho_d(\omega)$ and the corresponding Fano line shape (right) in the calculated transmission function $T(\omega)$ for the case of the z^2 orbital for the Co on Cu(001) system, discussed in detail in the following section. For both spectral and transmission functions, the resonance center is well-described by FF and FL fits. However, only the FF fit yields an accurate description of the flanks and the long-range decay. In the following, we will therefore use Eq. (13) to fit transmission functions.

IV. RESULTS

A. Co adatom on Cu(001) surface

The system under consideration is shown in the left panel of Fig. 4. A Cobalt atom is deposited at the hollow site of a Cu(001) surface. The Cu(001) surface is modeled by

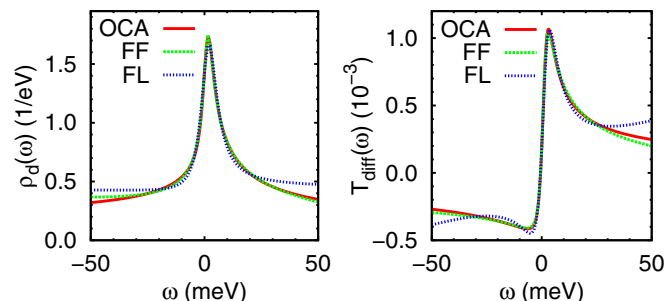


FIG. 3. (Color online) Fano-Lorentz (FL) and Fano-Frota (FF) fits of the impurity spectral function $\rho_d(\omega)$ (left) and the transmission function $T(\omega)$ (right) for z^2 -orbital, Co@Cu(001), $U = 2$ eV and $\epsilon_d = -1.0$ eV. See Sec. IV A for details.

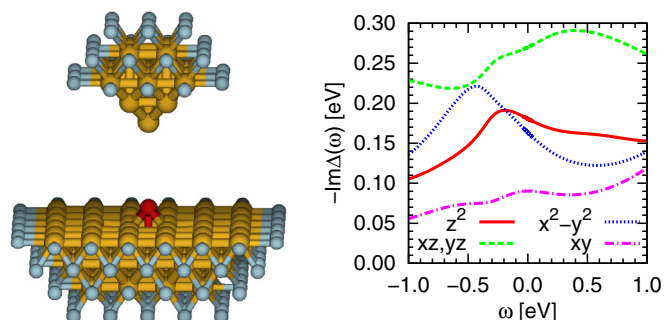


FIG. 4. (Color online) Left, geometry of the Co atom deposited on a Cu(001) surface; dark gray/red, Co; gray/yellow, Cu; light gray/blue, Bethe lattice. Right, imaginary part of the hybridization function for the Co 3d shell.

three Cu slabs of 36, 25, and 16 atoms, respectively, which are embedded into a Bethe lattice to describe the infinitely extended surface. We model the STM tip by a small pyramid of Cu atoms grown in the (001) direction, also embedded into a Bethe lattice. The tip is placed directly above the Co atom in a distance of 6 Å, so that the system is in the tunneling regime.

As explained in Sec. II we now compute the hybridization functions of the Co 3d orbitals (see right panel of Fig. 4). The fourfold symmetry of the Cu(001) surface leads to a splitting into four groups. The xz and yz orbitals are degenerate (in the following, results for the yz orbital are omitted) and exhibit the strongest hybridization at the Fermi level. The hybridization functions of z^2 and x^2-y^2 have comparable values around the Fermi level. The xy orbital has the lowest hybridization in the displayed energy window. All hybridization functions show a moderate energy dependence. Note that the hopping between different Co 3d orbitals is zero; i.e., they do not couple to each other on the single-particle level.

While the hybridization function is calculated *ab initio*, the Coulomb interaction U is used as a parameter that allows us to tune the Kondo coupling strength and explore the effect of the width of the Kondo peak on the transmission line shape. But in order to have an estimate of the magnitude, we have also calculated U *ab initio* for each of the d orbitals by constrained RPA calculations as described in Ref. [47]. We find values for U ranging from 1.8 to 2.6 eV [57]. Accordingly, we choose the U parameters to vary between 2 and 3 eV.

The hybridization functions from Fig. 4 together with the energy level ϵ_d and the effective Coulomb interaction U define an AIM, which is solved in the OCA [45]. It is a known issue of OCA that at too low temperatures (1–2 orders of magnitude below T_K) it gives rise to spurious non-Fermi liquid behavior and related artifacts in the impurity spectral function, leading to an overestimation of the height of the Kondo peak and an unphysical self-energy with positive imaginary part [58]. We circumvent this problem by lowering the temperature only to the point where the imaginary part of the self-energy becomes zero. At this point Fermi liquid behavior is obeyed, and the unitary limit of the Kondo peak is exactly recovered. Figure 5 shows impurity spectral functions $\rho_d(\omega)$ of the z^2 orbital for different values of the AIM parameters ϵ_d and U . For $\epsilon_d = -U/2$ (red solid and blue dotted curves) we have approximate particle-hole symmetry: the Kondo peak

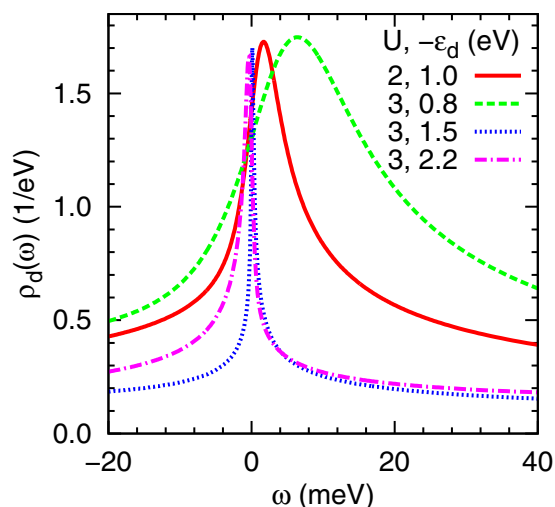


FIG. 5. (Color online) Impurity spectral functions for the z^2 orbital of Co@Cu(001) for different Anderson impurity model parameters U , ϵ_d .

is centered close to, but slightly above the Fermi level. Note that exact particle-hole symmetry is not achieved because of the nonconstant hybridization function. As expected, when U is increased the Kondo temperature and hence the width of the Kondo peak decrease strongly. On the other hand, detuning the system from particle-hole symmetry by shifting ϵ_d leads to a strong increase of the Kondo temperature due to charge fluctuations (green dashed, magenta dashed-dotted curves).

We now calculate the correlated transmission functions for Kondo peaks in different d orbitals. Figure 6 shows

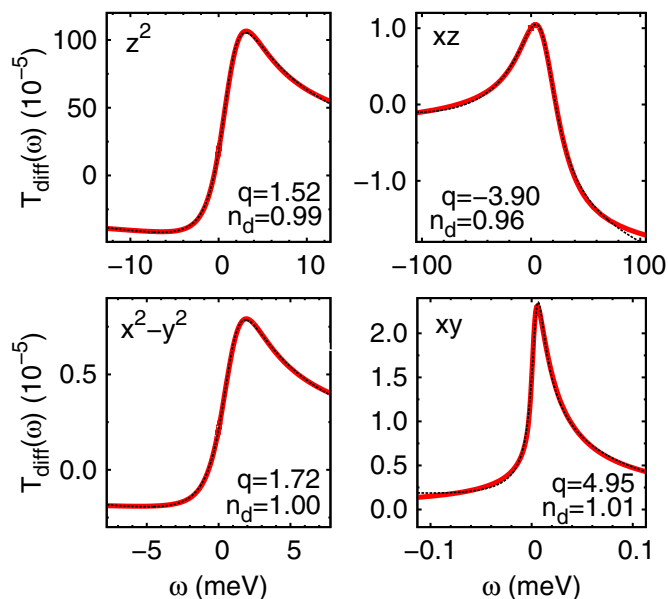


FIG. 6. (Color online) Transmission functions for different d orbitals of Co@Cu(001). Coulomb repulsion $U = 2$ eV, and energy level $\epsilon_d = -1$ eV (approximate particle-hole symmetry). The red continuous curves show the calculated transmission, the black dashed curves Fano-Frota fits. The transmission background has been subtracted [59].

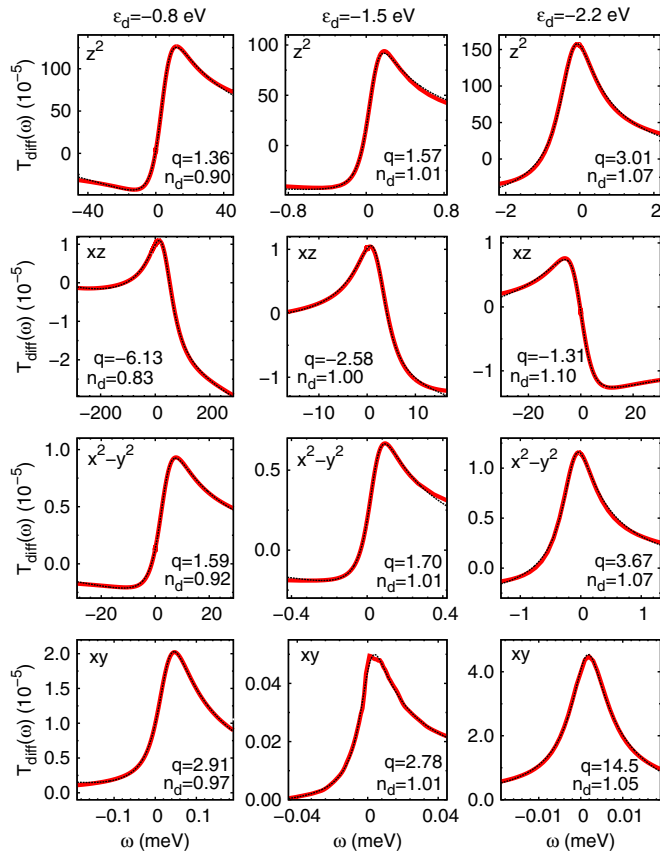


FIG. 7. (Color online) Transmission functions for different d orbitals of Co@Cu(001). Coulomb repulsion $U = 3$ eV vary occupation by shifting ϵ_d . The red continuous curves show the calculated transmission, the black dashed curves Fano-Frota fits. The transmission background has been subtracted [59].

transmission line shapes for different d orbitals for $U = 2$ eV and $\epsilon_d = -1.0$ eV. In order to make the features more clearly visible, here and in the following the transmission background was subtracted [59]. We find that the line shapes are indeed different for each orbital. We observe approximately antisymmetric Fano line shapes ($q \approx 1$) for z^2 and x^2-y^2 , and more peak-like features ($q \gg 1$) for xz and xy . In order to quantitatively describe the line shapes, we perform Frota fits to determine the q parameter and width of the line shapes, as explained in Sec. III. The z^2 and x^2-y^2 orbitals have comparable q values of 1.52 and 1.72, respectively. For xz , q becomes negative (-3.9) and for xy we find the most pronounced peak with $q = 4.95$. The width of the Fano features differs significantly, and in accordance with their hybridization strength at the Fermi level. Note that a feature with a very small width, as e.g., in the case of xy , might never be observed in an actual experiment, because of the Kondo temperature being much too low and because of limited resolution.

We now vary the Coulomb repulsion U and introduce charge fluctuations by shifting the d -level position ϵ_d , as can be seen in Fig. 7. When varying U , but maintaining particle-hole symmetry, the actual shape of the transmission features is only weakly affected, while the widths of the features change

strongly, as has already been seen and discussed for the spectral functions in Fig. 5. When introducing charge fluctuations, the Kondo peak becomes asymmetric (see Fig. 5). This asymmetry is also reflected in the transmission line shapes. We find that the q parameter consistently increases when ϵ_d is shifted downwards. For positive q (z^2 , x^2-y^2 , xy) lowering ϵ_d makes the line shapes more peak-like, while for negative q (xz), lowering ϵ_d leads to more dip-like line shapes.

Hence while the choice of AIM parameters U and ϵ_d does affect the transmission line shapes to some degree, it does not completely change its symmetry. For example, the sign of the q factor does not change.

While the signal width is determined by the hybridization and choice of AIM parameters exclusively, the signal amplitude decisively depends on the system geometry. Because we chose the z axis as our transport direction, a Kondo peak in the z^2 orbital results in a much more dominant feature compared to the remaining d orbitals, as can be seen in Figs. 6 and 7. Hence, if there is a Kondo peak in the z^2 orbital, the corresponding Fano feature will dominate in the transmission regardless of what happens in the other orbitals. Also, Fano features due to Kondo peaks in orbitals other than the z^2 orbital might be difficult to discern from the background if the background dispersion is strong compared to the Fano amplitudes. This statement remains true even if the STM tip is shifted laterally by moderate distances of a few Å. Although tunneling into orbitals other than z^2 becomes more favorable upon a lateral shift of the tip, the feature due to the Kondo peak in the z^2 remains the most dominant one.

B. Co adatom on Cu(111) surface

The next system we focus on is a Cobalt atom, deposited at the ‘‘hcp’’ hollow site of a Cu(111) surface, as can be seen in the left panel of Fig. 8. The surface is modeled by three Cu slabs of 27, 37, and 27 atoms, respectively, which are connected to a Bethe lattice. The tip is described by a Cu(111) pyramid, consisting of 10 copper atoms, also connected to a Bethe lattice. The threefold symmetry splits the five orbitals of the Co $3d$ shell into three groups: the nondegenerate z^2 orbital ($m = 0$) and two doubly degenerate groups, one with $m = \pm 1$ (xz and yz orbitals) and one with $m = \pm 2$ (xy and x^2-y^2 orbitals). The right panel of Fig. 8 shows the hybridization functions for each of the three groups. The group with the xz

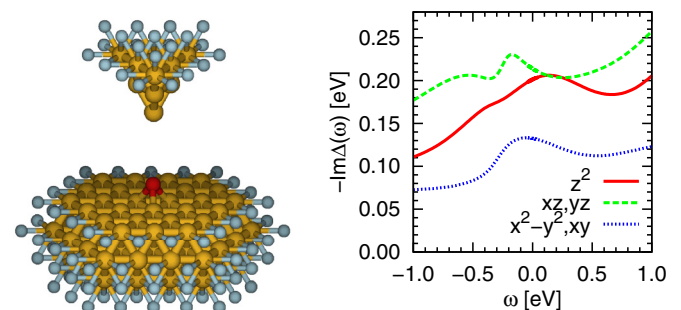


FIG. 8. (Color online) Left: Geometry of the Co atom deposited on a Cu(111) surface; dark gray/red, Co; gray/yellow, Cu; light gray/blue, Bethe lattice. Right: Imaginary part of the hybridization function of the Co $3d$ shell.

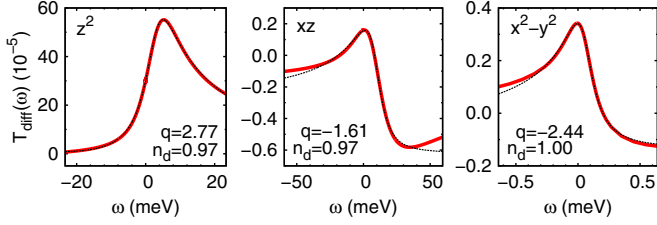


FIG. 9. (Color online) Transmission functions for different d orbitals of Co@Cu(111). Coulomb repulsion $U = 2$ eV, $\epsilon_d = -1.0$ eV. The red continuous curves show the calculated transmission, the black dashed curves Fano-Frota fits. The transmission background has been subtracted [59].

and yz orbitals exhibit the strongest hybridization at the Fermi level, the group with the x^2-y^2 and xy orbitals the weakest.

We proceed as described in the previous section and calculate transmission functions for the d orbitals of Co@Cu(111), assuming a Coulomb repulsion of $U = 2$ eV and (approximate) particle-hole-symmetry $\epsilon_d = -1.0$ eV (Fig. 9). Again, we find different line shapes for each orbital. The z^2 orbital gives the most peak-like transmission feature with $q = 2.77$, for x^2-y^2 we observe a transmission peak with a negative $q = -2.44$. The xz orbital results in a Fano-type feature with $q = -1.61$. The widths of the transmission features differ considerably, with the xz and yz orbitals having the largest width, and the xy and x^2-y^2 orbitals the lowest. The z^2 orbital again has the highest signal amplitude, as it couples strongly to the tip conduction electrons.

In Fig. 10, we calculate line shapes for different AIM parameters U and ϵ_d . We observe a similar behavior as for

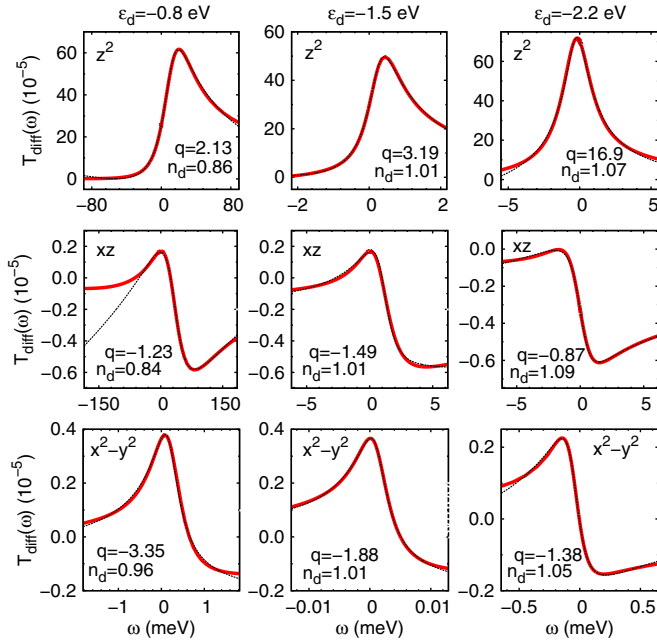


FIG. 10. (Color online) Transmission functions for different d orbitals of Co@Cu(111). Coulomb repulsion $U = 3$ eV vary occupation by shifting ϵ_d . The red continuous curves show the calculated transmission, the black dashed curves Fano-Frota fits. The transmission background has been subtracted [59].

Co@Cu(001). When staying in the particle-hole symmetric case and increasing U (middle column of Fig. 10), the line shapes remain similar, with slightly increased q values. We introduce charge fluctuations by shifting the position of ϵ_d (left and right column of Fig. 10). The q parameter increases when moving ϵ_d to lower energies. For positive q values, as for z^2 , this leads to more peak-like line shapes, while for negative q values, as for xz and x^2-y^2 , it leads to more fano- or dip-like line shapes. The only exception to this behavior occurs for the xz orbital, $U = 3$ eV and $\epsilon_d = -0.8$ eV. It has a very high Kondo temperature and equivalently wide Fano feature, and the Fano-Frota fit fails for negative energies. This suggests that the Fano line shape overlaps with other transmission features that alter the final line shape.

C. Temperature dependence and the occurrence of dips

The results presented so far are for the case of $T \rightarrow 0$ (according to the criterion discussed in Sec. IV A). We now study the temperature dependence of two line shapes: One tending toward a peak ($q > 1$) and one tending toward a dip ($q < 1$). We pick the xz orbital of Co@Cu(111), $U = 3$ eV, $\epsilon_d = -1.5$ eV ($q = -1.49$), and $\epsilon_d = -2.2$ eV ($q = -0.87$), respectively. The top row of Fig. 11 shows the evolution of the aforementioned two line shapes. For increasing temperature, the signal amplitude diminishes, while its width grows. The peak does not decay symmetrically. The “peak” component of the Fano feature decays faster than the “dip” component of the feature, so that, in both cases, the feature as a whole becomes increasingly dip-like with increasing temperature. In order to quantify that, we perform Fano-Frota fits and calculate the q parameter. We find that the q parameter decreases considerably

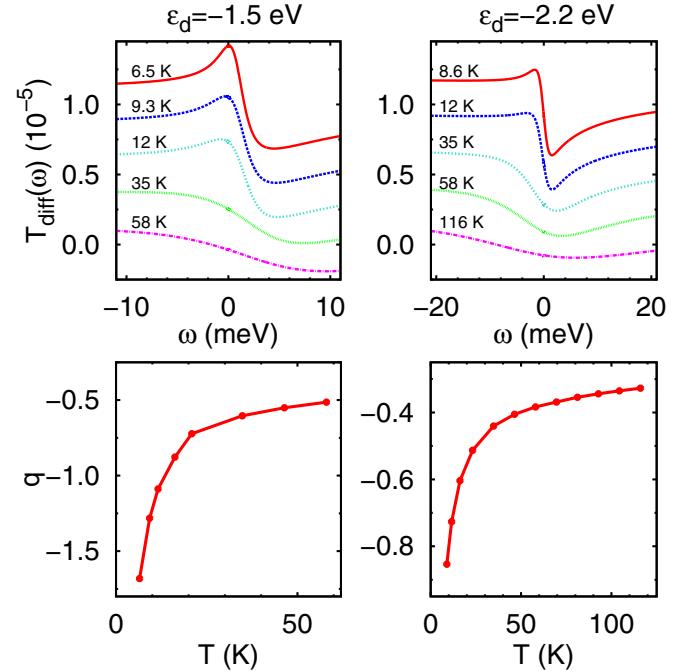


FIG. 11. (Color online) Temperature dependence of two different line shapes for Co@Cu(111), xz , $U = 3$ eV, $\epsilon_d = -1.5$ eV, and $\epsilon_d = -2.2$ eV, respectively. Top: Transmission. Bottom: q parameter; the lines are a guide for the eye.

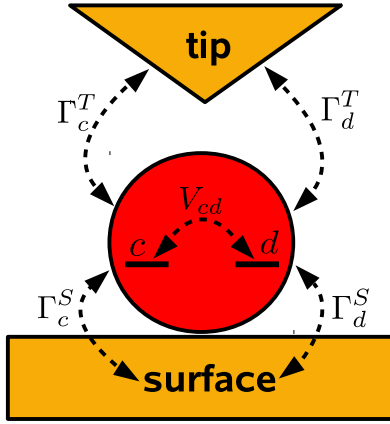


FIG. 12. (Color online) Sketch of the simplified model. The effective atom A is described by the correlated d level and one conduction electron level c , in contact with the surface and the tip.

when temperature is rising, irrespective if the feature tends more toward peak or dip in the $T \rightarrow 0$ case.

V. A SIMPLIFIED MODEL

The interference mechanism leading to different Fano line shapes still is a matter of discussion [23–30,60,61]. We expand on this discussion by introducing a simple model that allows us to determine transmission line shapes from *ab initio* parameters. Figure 12 shows a schematic drawing of our model system. The central assumption is that the quantum interference primarily occurs on the magnetic adatom, namely between one s -type and/or p -type level (in the following, we will simply call it the conduction level c) and the correlated d level. Both levels are in contact to the tip T and the surface S, and the respective interactions are taken into account by coupling matrices $\Gamma_{T/S}$. As a second central assumption we neglect the direct tunneling from the tip to the surface.

The starting point of our model is the correlated Green's function of the effective atom comprising the conduction c level and the correlated d level of the magnetic atom:

$$G_A(\omega) = [\omega \hat{P}_A - \hat{H}_A - \hat{\Delta}(\omega) - \Sigma_d(\omega) \hat{P}_d]^{-1} = \begin{pmatrix} \omega - \epsilon_c - \Delta_c(\omega) & -V_{cd} - \Delta_{cd}(\omega) \\ -V_{dc} - \Delta_{dc}(\omega) & \omega - \epsilon_d - \Delta_d(\omega) - \Sigma_d(\omega) \end{pmatrix}^{-1} \quad (14)$$

\hat{P}_A is a projector onto the effective atom A, while \hat{P}_d projects onto the d level only. All parameters can either be extracted from the KS calculation (ϵ_d , ϵ_c , V_{cd} , $\hat{\Delta}(\omega)$) or from the OCA calculation ($\Sigma_d(\omega)$), while the chemical potential has been set to zero $\mu = 0$. The diagonal elements of the hybridization function $\hat{\Delta}(\omega)$ lead to a shift (real part) of the level position of ϵ_c and ϵ_d , respectively, and yield an effective level broadening (imaginary part). Also note that the hybridization function has off-diagonal components $\Delta_{cd}(\omega) = \Delta_{dc}(\omega)$, which can be understood as an additional hopping between the c and d level mediated by hoppings via

the substrate, to give a total effective coupling of $\tilde{V}_{cd} = V_{cd} + \Delta_{cd}$. The coupling matrices $\Gamma_{S/T}(\omega)$ necessary for calculating the transmission function by Eq. (6) can be obtained by decomposing the hybridization function into a tip ($\Delta_T(\omega)$) and a surface ($\Delta_S(\omega)$) component and taking the imaginary parts, i.e., $\Gamma_{S/T}(\omega) = -2 \text{Im} \Delta_{S/T}(\omega)$.

For the conduction level c of the effective atom we choose the s or p orbital that couples to the correlated d orbital. In the case of the (001) and the (111) substrates the z^2 orbital couples to the s as well as the p_z orbital. In this case we apply a unitary transformation in the subspace of the s and p_z orbitals such that the z^2 orbital decouples completely from one of the orbitals in the new basis. The sp_z -hybridized orbital coupling to the z^2 is then found to be the linear combination $|sp_z\rangle \propto \tilde{V}_{sz^2}|s\rangle + \tilde{V}_{pz^2}|p_z\rangle$, where \tilde{V}_{sz^2} and \tilde{V}_{pz^2} are the effective hoppings of the z^2 orbital with the s and p_z orbitals, respectively. On both surfaces, the xz orbital couples to p_x and the yz orbital to p_y . For the (001) surface both the x^2-y^2 and the xy orbitals do not interact with any of the s or p orbitals on the atom, while on the (111) surface, they do interact with the p_y and p_x orbitals, respectively.

In Figs. 13 and 14, we compare line shapes calculated for the simplified model with the full *ab initio* results from Sec. IV. For the Co@Cu(001) surface, the simplified model consisting of the z^2 orbital and the sp_z -hybridized orbital reproduces the line shape of the z^2 orbital quite well. Only the peak character is slightly overestimated. In the case of the xz orbital the line shape of the simplified model including the p_x orbital is in excellent agreement with that of the full *ab initio* calculation. For the x^2-y^2 orbital the agreement between the simplified model and the full calculation is not as good. As stated before this orbital does not interact with any s or p orbital

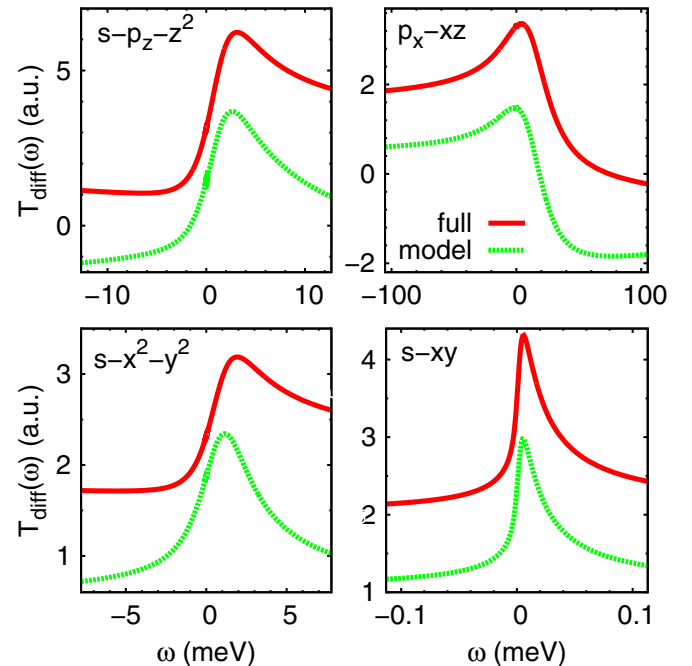


FIG. 13. (Color online) Transmissions calculated *ab initio* with the ANT.G package (see Sec. IV) and for the simplified model; Co@Cu(001), $U = 2$ eV, $\epsilon_d = -1$ eV. The transmission functions are rescaled and offset for better visibility.

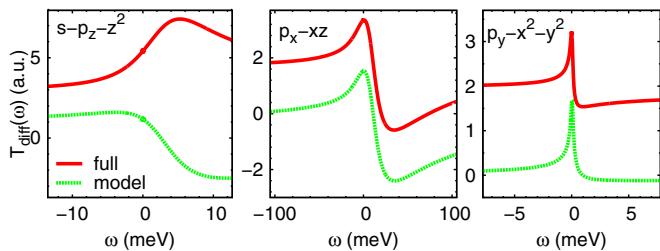


FIG. 14. (Color online) Transmissions calculated *ab initio* with the ANT.G package (see Sec. IV) and for the simplified model; Co@Cu(111), $U = 2$ eV, $\epsilon_d = -1$ eV. The transmission functions are rescaled and offset for better visibility.

on the Co atom. Hence, the transmission of the simplified model reproduces simply the Kondo peak in the spectral function since no interference is taking place. On the other hand, the full transmission shows a somewhat asymmetric Fano feature ($q \approx 1.7$), indicating that interference with some substrate state(s) must take place, which is not included in the model. Finally, for the xy orbital we find very good agreement between the simplified model and the full calculation. The line shape in both calculations simply reproduces the Kondo peak in the spectral function of the xy orbital, indicating the absence of any interference effects between this d level and s and p levels on the atoms as well as substrate states.

We find a somewhat similar picture for Co@Cu(111). For the xz orbital the model including the interaction with the p_x orbital gives a line shape in excellent agreement with the full calculation. Also for the x^2-y^2 the simplified model including the p_y orbital on the atom reproduces the line shape of the full calculation very well. However, in the case of the z^2 orbital the simplified model including the sp_z -hybridized orbital fails quite badly in reproducing the line shape of the full calculation. Apparently, interference with tunneling paths to substrate states play an important role here.

VI. DISCUSSION

For Co@Cu(001), we found transmission line shapes ranging from asymmetric Fano features with positive (z^2 , x^2-y^2) and negative (xz) q values to a more peak-like feature (xy). The line shapes are determined by the interference of different tunneling paths. Our simplified model calculations indicate that for z^2 and xz the interference takes place on the adatom between the correlated d level and the noninteracting sp levels coupling to the d orbital. For the xy orbital, no interference occurs between the conduction and impurity tunneling channels. Hence, one directly observes the shape of the Kondo peak in the transmission. On the other hand, for the x^2-y^2 orbital, the interference mechanism probably involves the Cu substrate states, which are not captured by the simplified model. Experimentally, asymmetric Fano line shapes were reported with $q \sim 1.1-1.2$ in the tunneling regime [12,18]. The measured line shapes are comparable to the features we found both in the z^2 and x^2-y^2 orbitals (see Figs. 6 and 7), although the z^2 orbital yields a slightly

better agreement. Better agreement with experiment can surely be achieved by adjusting the Anderson model parameters and fitting the calculated spectra with the experimental ones. We would like to stress though that finding good agreement with experiment is not the primary goal of this work, but rather to demonstrate how different orbital symmetries give rise to different Fano-Kondo line shapes. A recent study by one of us [47] found an under-screened Kondo effect for Co@Cu(001), where the z^2 and x^2-y^2 are nearly half filled, but only the z^2 orbital is Kondo screened at finite temperatures due to its higher Kondo temperature. Reference [31] comes to similar conclusions, finding a Kondo peak in the z^2 orbital with $q = 1.2$ in the tunneling regime and explaining it due to the interference of the z^2 with the s orbital.

For Co@Cu(111), we found asymmetric to peak-like Fano line shapes with positive (z^2) and negative (xz , x^2-y^2) q values. For the latter two, we can understand the tunneling interference in terms of the model presented in the previous section. The interference occurs on the magnetic atom, between the conduction electron channel, modeled by one of the p orbitals, and the respective d level. For z^2 , which is interacting with the sp_z hybridized level, our model fails, indicating that interference with substrate states plays an important role here.

Experimentally, dips were reported with q values close to zero [11,12,32], which does not seem to agree with any of the calculated line shapes. The z^2 orbital, aligned in the transport direction, again shows the strongest signal, but is rather peak-like. The closest candidate to a dip-like line shape is the xz orbital, particularly when increasing the occupancy relative to half-filling by moving the d -level position downward in energy (see Fig. 10). In Sec. IV C, we studied its temperature dependence, and found that the line shape became increasingly dip-like when increasing temperature. However, note that in our calculations for the xz orbitals we find $q < 0$ while in experiment q is always positive.

Probably, the surface state of the Cu(111) surface [62] plays an important role for determining the line shape [11,25,30,63], since its tunneling amplitude may be twice as strong compared to tunneling into bulk states [64]. However, our embedded cluster calculation probably does not capture the surface state properly. The importance of the surface state for reproducing the correct line shape in the Co@Cu(111) system is also stressed in Ref. [31], where the surface state is not properly captured and the correct q value could not be reproduced either.

VII. CONCLUSIONS

In summary, we have calculated the orbital signatures of Kondo peaks in the STM spectra of transition metal adatom systems, namely Co@Cu(001) and Co@Cu(111). Our calculations show that the measured line shapes allow us to draw some conclusions on the d orbital(s) involved in the Kondo effect since the line shape depends to a large extent on the coupling of the d orbital to the sp orbitals on the adatom, which in turn is determined by the orbital symmetry. However, also temperature, effective interaction U , and in particular the occupancy of the d orbital have a strong influence on the actual

line shapes. Also, if multiorbital effects are important for the actual shape of a Fano-Kondo feature, this approach per se is not appropriate. Nevertheless, even in the case of a multiorbital Kondo effect, often one orbital will be dominant in the tunnel spectra. In fact, if a Kondo resonance forms in the z^2 orbital, the corresponding Fano feature will be dominant in the tunnel spectrum for the typical case of an s -type STM tip, so that Kondo features coming from other d orbitals are likely not visible. These results are also relevant for STS of transition metal complexes on metallic substrates [65–67], maybe even more so since tunneling into surface states is less important there.

We stress that the here developed method can in principle also be applied to the contact regime. However, unlike in the tunneling case, in the contact regime the voltage can no longer be assumed to mainly drop between tip and adatom. Rather, the voltage drop will distribute in some way over the contact according to the actual geometry of the contact region [67] and needs to be calculated or estimated. Moreover, the actual contact geometry is probably also relevant for the coupling between d orbitals and conduction electrons and thus also has a strong influence on the line shapes. Therefore, possible contact geometries need to be explored and relaxed with some care.

Based on our results, we propose a poor man's method to obtain information on the orbital(s) involved in the Kondo effect measured in an actual experiment solely on the basis of a density functional theory calculation of the system: by tailoring an appropriate self-energy for each orbital such that the width of the resulting Kondo peak in that orbital reproduces the width of the measured Fano-Kondo line shape, one can calculate the corresponding line shapes and compare to experiment.

ACKNOWLEDGMENTS

We acknowledge fruitful discussions with R. Requist, M. Karolak, and J. J. Palacios.

APPENDIX: COMPLEX AND REAL FANO LINE SHAPES

Here we derive the real Fano line shape given by Eq. (11) from its complex representation in Eq. (10):

$$\rho_{\text{FL}}(\omega) = \text{Im} \left[e^{i\phi_q} \left(\frac{A}{\omega - \omega_0 + i\Gamma} \right) \right]. \quad (\text{A1})$$

Introducing the abbreviation $\epsilon = (\omega - \omega_0)/\Gamma$, we have

$$\begin{aligned} \rho_{\text{FL}} &= \frac{A}{\Gamma} \cdot \text{Im} \left[(\cos(\phi_q) + i \sin(\phi_q)) \frac{\epsilon - i}{\epsilon^2 + 1} \right] \\ &= \frac{A}{\Gamma} \left[\frac{-\cos(\phi_q) + \epsilon \sin(\phi_q)}{\epsilon^2 + 1} \right] \\ &= \frac{A}{\Gamma} \left[\frac{-\cos^2\left(\frac{\phi_q}{2}\right) + \sin^2\left(\frac{\phi_q}{2}\right) + 2\epsilon \sin\left(\frac{\phi_q}{2}\right) \cos\left(\frac{\phi_q}{2}\right)}{\epsilon^2 + 1} \right] \\ &= \frac{A}{\Gamma} \left[\frac{-1 + \tan^2\left(\frac{\phi_q}{2}\right) + 2\epsilon \tan\left(\frac{\phi_q}{2}\right)}{\epsilon^2 + 1} \right] \cos^2\left(\frac{\phi_q}{2}\right). \end{aligned}$$

Defining $q \equiv \tan(\phi_q/2)$, we arrive at

$$\rho_{\text{FL}} = \frac{A}{\Gamma} \left[\frac{(q + \epsilon)^2}{\epsilon^2 + 1} - 1 \right] \frac{1}{1 + q^2}, \quad (\text{A2})$$

which is the same as Eq. (11).

-
- [1] A. Hewson, *The Kondo Problem to Heavy Fermions*, edited by D. Edwards and D. Melville (Cambridge University Press, Cambridge, 1997).
- [2] W. de Haas, J. de Boer, and G. van den Berg, *Physica* **1**, 1115 (1934).
- [3] M. P. Sarachik, E. Corenzwit, and L. D. Longinotti, *Phys. Rev.* **135**, A1041 (1964).
- [4] J. Kondo, *Prog. Theor. Phys.* **32**, 37 (1964).
- [5] A. Posazhennikova, B. Bayani, and P. Coleman, *Phys. Rev. B* **75**, 245329 (2007).
- [6] N. Roch, S. Florens, V. Bouchiat, W. Wernsdorfer, and F. Balestro, *Nature* **453**, 633 (2008).
- [7] J. Nygard, D. H. Cobden, and P. E. Lindelof, *Nature* **408**, 342 (2000).
- [8] P. Jarillo-Herrero, J. Kong, H. S. van der Zant, C. Dekker, L. P. Kouwenhoven, and S. De Franceschi, *Nature* **434**, 484 (2005).
- [9] J. Li, W.-D. Schneider, R. Berndt, and B. Delley, *Phys. Rev. Lett.* **80**, 2893 (1998).
- [10] V. Madhavan, W. Chen, T. Jamneala, M. F. Crommie, and N. S. Wingreen, *Science* **280**, 567 (1998).
- [11] H. C. Manoharan, C. P. Lutz, and D. M. Eigler, *Nature* **403**, 512 (2000).
- [12] N. Knorr, M. A. Schneider, L. Diekhöner, P. Wahl, and K. Kern, *Phys. Rev. Lett.* **88**, 096804 (2002).
- [13] K. Nagaoka, T. Jamneala, M. Grobis, and M. F. Crommie, *Phys. Rev. Lett.* **88**, 077205 (2002).
- [14] A. J. Heinrich, J. A. Gupta, C. P. Lutz, and D. M. Eigler, *Science* **306**, 466 (2004).
- [15] A. Zhao, Q. Li, L. Chen, H. Xiang, W. Wang, S. Pan, B. Wang, X. Xiao, J. Yang, J. G. Hou, and Q. Zhu, *Science* **309**, 1542 (2005).
- [16] M. F. Crommie, *Science* **309**, 1501 (2005).
- [17] V. Iancu, A. Deshpande, and S.-W. Hla, *Phys. Rev. Lett.* **97**, 266603 (2006).
- [18] N. Néel, J. Kröger, L. Limot, K. Palotas, W. A. Hofer, and R. Berndt, *Phys. Rev. Lett.* **98**, 016801 (2007).
- [19] U. Fano, *Phys. Rev.* **124**, 1866 (1961).
- [20] H. Prüser, M. Wenderoth, A. Weismann, and R. G. Ulbrich, *Phys. Rev. Lett.* **108**, 166604 (2012).
- [21] H. O. Frota and L. N. Oliveira, *Phys. Rev. B* **33**, 7871 (1986).
- [22] H. O. Frota, *Phys. Rev. B* **45**, 1096 (1992).
- [23] M. Plihal and J. W. Gadzuk, *Phys. Rev. B* **63**, 085404 (2001).
- [24] V. Madhavan, W. Chen, T. Jamneala, M. F. Crommie, and N. S. Wingreen, *Phys. Rev. B* **64**, 165412 (2001).

- [25] C.-Y. Lin, A. H. Castro Neto, and B. A. Jones, *Phys. Rev. Lett.* **97**, 156102 (2006).
- [26] O. Újsághy, J. Kroha, L. Szunyogh, and A. Zawadowski, *Phys. Rev. Lett.* **85**, 2557 (2000).
- [27] A. Schiller and S. Hershfield, *Phys. Rev. B* **61**, 9036 (2000).
- [28] P. Wahl, L. Diekhöner, M. A. Schneider, L. Vitali, G. Wittich, and K. Kern, *Phys. Rev. Lett.* **93**, 176603 (2004).
- [29] J. Merino and O. Gunnarsson, *Phys. Rev. B* **69**, 115404 (2004).
- [30] J. Merino and O. Gunnarsson, *Phys. Rev. Lett.* **93**, 156601 (2004).
- [31] P. P. Baruselli, R. Requist, A. Smogunov, M. Fabrizio, and E. Tosatti, *Phys. Rev. B* **92**, 045119 (2015).
- [32] L. Vitali, R. Ohmann, S. Stepanow, P. Gambardella, K. Tao, R. Huang, V. S. Stepanyuk, P. Bruno, and K. Kern, *Phys. Rev. Lett.* **101**, 216802 (2008).
- [33] N. Néel, J. Kröger, and R. Berndt, *Phys. Rev. B* **82**, 233401 (2010).
- [34] D.-J. Choi, M. V. Rastei, P. Simon, and L. Limot, *Phys. Rev. Lett.* **108**, 266803 (2012).
- [35] D. Jacob and J. J. Palacios, *J. Chem. Phys.* **134**, 044118 (2011).
- [36] W. Kohn and L. J. Sham, *Phys. Rev.* **140**, A1133 (1965).
- [37] C. J. Slater, *The Self-Consistent Field for Molecular and Solids*, Quantum Theory of Molecular and Solids, Vol. 4 (McGraw-Hill, New York, 1974).
- [38] S. H. Vosko, L. Wilk, and M. Nusair, *Can. J. Phys.* **58**, 1200 (1980).
- [39] W. J. Hehre, R. F. Stewart, and J. A. Pople, *J. Chem. Phys.* **51**, 2657 (1969).
- [40] J. B. Collins, P. von R. Schleyer, J. S. Binkley, and J. A. Pople, *J. Chem. Phys.* **64**, 5142 (1976).
- [41] P. J. Hay and W. R. Wadt, *J. Chem. Phys.* **82**, 270 (1985).
- [42] W. R. Wadt and P. J. Hay, *J. Chem. Phys.* **82**, 284 (1985).
- [43] P. J. Hay and W. R. Wadt, *J. Chem. Phys.* **82**, 299 (1985).
- [44] H. A. Bethe, *Proc. Roy. Soc. London A: Math. Phys. Eng. Sci.* **150**, 552 (1935).
- [45] K. Haule, S. Kirchner, J. Kroha, and P. Wölfle, *Phys. Rev. B* **64**, 155111 (2001).
- [46] D. Jacob, K. Haule, and G. Kotliar, *Phys. Rev. Lett.* **103**, 016803 (2009).
- [47] D. Jacob, *J. Phys. Condens. Matter* **27**, 245606 (2015).
- [48] P. W. Anderson, *Phys. Rev.* **124**, 41 (1961).
- [49] C. Caroli, R. Combescot, D. Lederer, P. Nozieres, and D. Saint-James, *J. Phys. C* **4**, 2598 (1971).
- [50] R. Landauer, *IBM J. Res. Dev.* **1**, 223 (1957).
- [51] S. Datta, *Electronic Transport in Mesoscopic Systems* (Cambridge University Press, Cambridge, 1995), Cambridge Books Online.
- [52] Y. Meir and N. S. Wingreen, *Phys. Rev. Lett.* **68**, 2512 (1992).
- [53] M. H. Hettler, J. Kroha, and S. Hershfield, *Phys. Rev. B* **58**, 5649 (1998).
- [54] C. A. Balseiro, M. J. Usaj, and G. Sánchez, *J. Phys. Condens. Matter* **22**, 425602 (2010).
- [55] P. Roura-Bas, *Phys. Rev. B* **81**, 155327 (2010).
- [56] H. Prüser, M. Wenderoth, P. E. Dargel, A. Weismann, R. Peters, T. Pruschke, and R. G. Ulbrich, *Nat. Phys.* **7**, 203 (2011).
- [57] More specifically, we obtain 1.80 eV for the z^2 orbital, 1.78 eV for the xz and yz orbitals, 1.81 eV for the x^2-y^2 orbital, and 2.59 eV for the xy orbital.
- [58] T. A. Costi, J. Kroha, and P. Wölfle, *Phys. Rev. B* **53**, 1850 (1996).
- [59] The background is calculated by calculating the transmission function without adding the self-energy but pushing the respective d level away from the Fermi level.
- [60] H. G. Luo, T. Xiang, X. Q. Wang, Z. B. Su, and L. Yu, *Phys. Rev. Lett.* **92**, 256602 (2004).
- [61] R. Žitko and T. Pruschke, *New J. Phys.* **12**, 063040 (2010).
- [62] M. F. Crommie, C. P. Lutz, and D. M. Eigler, *Nature* **363**, 524 (1993).
- [63] A. Bogicevic, S. Ovesson, P. Hylgaard, B. I. Lundqvist, H. Brune, and D. R. Jennison, *Phys. Rev. Lett.* **85**, 1910 (2000).
- [64] O. Jeandupeux, L. Bürgi, A. Hirstein, H. Brune, and K. Kern, *Phys. Rev. B* **59**, 15926 (1999).
- [65] D. Jacob, M. Soriano, and J. J. Palacios, *Phys. Rev. B* **88**, 134417 (2013).
- [66] J. Kügel, M. Karolak, J. Senkpiel, P.-J. Hsu, G. Sangiovanni, and M. Bode, *Nano Lett.* **14**, 3895 (2014).
- [67] S. Karan, D. Jacob, M. Karolak, C. Hamann, Y. Wang, A. Weismann, A. I. Lichtenstein, and R. Berndt, *Phys. Rev. Lett.* **115**, 016802 (2015).